J Neurophysiol 115: 2937–2949, 2016.
First published March 23, 2016; doi:10.1152/jn.00671.2015.

Biophysical constraints on lateral inhibition in the olfactory bulb

Alexa B. R. McIntyre[1] and Thomas A. Cleland[2]
[1]*Tri-Institutional Program in Computational Biology and Medicine, Cornell University, Ithaca, New York; and* [2]*Department of Psychology, Cornell University, Ithaca, New York*

Submitted 7 July 2015; accepted in final form 16 March 2016

McIntyre AB, Cleland TA. Biophysical constraints on lateral inhibition in the olfactory bulb. *J Neurophysiol* 115: 2937–2949, 2016. First published March 23, 2016; doi:10.1152/jn.00671.2015.—The mitral cells (MCs) of the mammalian olfactory bulb (OB) constitute one of two populations of principal neurons (along with middle/deep tufted cells) that integrate afferent olfactory information with top-down inputs and intrinsic learning and deliver output to downstream olfactory areas. MC activity is regulated in part by inhibition from granule cells, which form reciprocal synapses with MCs along the extents of their lateral dendrites. However, with MC lateral dendrites reaching over 1.5 mm in length in rats, the roles of distal inhibitory synapses pose a quandary. Here, we systematically vary the properties of a MC model to assess the capacity of inhibitory synaptic inputs on lateral dendrites to influence afferent information flow through MCs. Simulations using passivized models with varying dendritic morphologies and synaptic properties demonstrated that, even with unrealistically favorable parameters, passive propagation fails to convey effective inhibitory signals to the soma from distal sources. Additional simulations using an active model exhibiting action potentials, subthreshold oscillations, and a dendritic morphology closely matched to experimental values further confirmed that distal synaptic inputs along the lateral dendrite could not exert physiologically relevant effects on MC spike timing at the soma. Larger synaptic conductances representative of multiple simultaneous inputs were not sufficient to compensate for the decline in signal with distance. Reciprocal synapses on distal MC lateral dendrites may instead serve to maintain a common fast oscillatory clock across the OB by delaying spike propagation within the lateral dendrites themselves.

olfaction; computational neuroscience; lateral dendrites; cable theory; mitral cell

THE EXTERNAL PLEXIFORM LAYER (EPL) of the mammalian olfactory bulb (OB) mediates recurrent and lateral inhibition of OB principal neurons (mitral and middle/deep tufted cells) via their synaptic interactions with granule cell (GC) interneurons. The extensive lateral dendrites of mitral cells (MCs) develop closely adjoining reciprocal synapses with spines on the perpendicularly-oriented dendrites of GCs. In studies of synaptic physiology in the OB, it is clear that GC spines can deliver graded recurrent inhibition onto MC dendrites following MC excitation without the need for GC somatic spiking (Isaacson and Strowbridge 1998; Schoppa et al. 1998), although the efficacy and functional utility of graded vs. GC spike-mediated inhibition in the intact system remain open questions. Foundational work in the OB originally concluded that EPL lateral inhibition, based on the assumption of a distance-dependent topology of synaptic weights, mediated similarity-dependent contrast enhancement (e.g., Yokoi et al. 1995). This hypothesis arose in part by simple analogy with the retina, although the high stimulus dimensionality generated by the olfactory epithelium coupled with the lack of an external physical metric akin to wavelength or frequency rules out this possibility (Cleland 2014; Cleland and Sethupathy 2006). In accordance with the latter theoretical work, subsequent experimental studies clearly demonstrated the absence of nearest-neighbor topologies of either chemoreceptive field similarity (Soucy et al. 2009) or lateral inhibitory weights in OB EPL circuitry (Fantana et al. 2008). While it is becoming increasingly clear that learning, mediated at least in part by the selective survival and differentiation of adult-generated GCs, underlies the architecture of lateral inhibition across the EPL (Arruda-Carvalho et al. 2014; Lepousez et al. 2013; Tong et al. 2014), this still begs the question of what mechanisms map and regulate the topology of inhibition in the EPL. To address these questions at a functional level, the biophysical constraints of the underlying physical system first must be established.

Somatofugal spikes actively propagate along the full extent of MC lateral dendrites (Christie and Westbrook 2003; Debarbieux et al. 2003; Xiong and Chen 2002), which extend and branch sufficiently to reach nearly any point within the EPL (Orona et al. 1984; Shipley and Ennis 1996). Thus physical distance need not be a factor in estimating the density or efficacy of MC-to-GC synaptic connections. In contrast, synaptic inhibition does not actively propagate. The centripetal axis of propagation in OB principal neurons passes from the apical dendrite sampling the glomerulus, through the soma, to the axon and its targets in other olfactory structures, with spike initiation in the soma or apical dendrite (Chen et al. 2002). Given that this axis bypasses the lateral dendrites, inhibitory inputs to these dendrites must affect cellular state at the soma to influence the information throughput of MCs by altering the timing of centripetally propagating spikes. If inhibitory synapses that contact MC dendrites at distal locations are physically unable to meaningfully affect signal propagation through MCs, this would favor models of EPL function based on proximity-independent lateral excitation of GCs by MCs coupled with proximity-dependent lateral inhibition of MCs by GCs (McTavish et al. 2012), and sharply restrict the plausible hypotheses regarding how learning and other factors can shape the distribution of functional lateral inhibition across the EPL.

We constructed biophysically detailed microcircuit models of GC-MC interactions, based on the MC model of Li and Cleland (2013), to assess the capacities of inhibitory synaptic inputs delivered onto lateral dendrites to modify MC state at the soma. First, using a passive version of the model to measure cable properties, we measured the effects of four interacting variables on both polarization and shunting effects at the soma that could impede or delay action potential prop-

Address for reprint requests and other correspondence: T. A. Cleland, Dept. of Psychology, Cornell Univ., 278E Uris Hall, Ithaca, NY 14853 (e-mail: tac29@cornell.edu).

agation. Specifically, these included *1*) the distance between a synaptic input and the soma; *2*) the peak synaptic conductance; *3*) the chloride reversal potential (ECl) that governs the driving force through the $GABA_A$ receptor; and *4*) the dendritic diameter. We also separately assessed two tapering models of the lateral dendrite and the effects of dendritic branching. Second, we used an active version of the model, incorporating the more realistically tapering dendrite and exhibiting subthreshold oscillations (STOs), bursting, and other dynamic MC properties, to measure the effects of lateral inhibitory inputs on spike propagation and timing. The results of our simulations suggest that distal inhibitory inputs are ineffective at modifying the state of the primary MC axis sufficiently to delay or otherwise affect action potential generation or centripetal propagation. In contrast, perisomatic inhibition constrained the STO phase window of MC action potential firing, particularly when strong enough to reflect multiple synchronous synaptic inputs. Such phase regulation of spike timing in resonant neurons has been shown to enhance spike synchrony within an appropriately coupled OB network (Li and Cleland 2013).

MATERIALS AND METHODS

Simulator

All simulations were performed using NEURON 7.3 (http://www.neuron.yale.edu) running on Linux Ubuntu 14.04 LTS. A fixed time step of $dt = 0.01$ ms was used for all simulations.

Mitral Cell Morphology

We adapted the MC model of Li and Cleland (2013) for use in these studies. The cell model includes a cylindrical, isometric soma (length = 25 μm, diameter = 20 μm), an apical (primary) dendrite (length = 370 μm, diameter = 3.5 μm) with a glomerular tuft (length = 20 μm, diameter = 0.5 μm), and a single, multicompartmental lateral (secondary) dendrite. The lateral dendrite was the region of interest in this study; its properties were systematically varied. As in the model of origin, the membrane resistivity in all models was 30 k$\Omega\cdot$cm^2. Somatic input resistance ranged from 182 MΩ in the models with the thinnest lateral dendrites to 93 MΩ in the models with the thickest lateral dendrites, all within a physiological range described as 88–280 MΩ by Desmaisons et al. (1999). The specific membrane capacitance was 1.2 μF/cm^2.

Axial Resistivity

The axial resistivity R_a of the lateral dendrite is a critical parameter, as it affects length constants (the efficacy of passive voltage propagation along cables) as effectively as the dendritic diameter, a variable of interest. We determined R_a according to experimental measurements of MC dendritic length constants by Djurisic et al. (2004). Specifically, Djurisic et al. (2004) estimated a length constant of 1,246 $\pm$ 217 μm in MC apical dendrites with an average diameter of 4.0 μm. Rounding this estimate to 1,200 μm, and using the resistivity variant of the length constant equation,

$$\lambda = \sqrt{\frac{R_m \cdot d}{4R_a}} \quad (1)$$

where λ denotes the length constant in cm, R_m is the membrane resistivity in $\Omega\cdot$cm^2, d is the dendritic diameter in cm, and R_a is the axial resistivity in $\Omega\cdot$cm, we solved for the axial resistivity R_a such that $R_a = 208$ $\Omega\cdot$cm. This value then was used in all simulations reported herein.

We extended the estimates of Djurisic et al. (2005) to the lateral dendrite, which is valid assuming that R_m and R_a are similar in the apical and lateral dendrites. By *Eq. 1*, the length constant of a 0.5-μm dendrite is 425 μm, that of a 2.0-μm dendrite is 849 μm, and that of a 3.4-μm dendrite is 1,107 μm. Notably, the attenuating effects of these length constants in the model closely matched empirical data. Specifically, a spike waveform generated in the model soma was attenuated by a factor of ~0.33 at 179-μm distance along a nonlinearly tapered dendrite in which the fast sodium current had been blocked (Fig. 1, NLT). A spike waveform command potential inserted into a MC in the presence of tetrodotoxin to block spike propagation was attenuated by a comparable factor at a comparable distance (Fig. 8 in Djurisic et al. 2004).

Properties of the Passivized Model

For cable-theoretic simulations of the propagation of inhibitory synaptic effects to the soma, we "passivized" the MC model of Li and Cleland (2013) by rendering all membrane conductances ohmic with conductances equal to those of the active model at rest. That is, the cell was in a state identical to that of the fully active model at rest, but the gating variables of the active membrane conductances did not change when the cell was perturbed. For simplicity, we implemented this state by reparameterizing a single, ohmic, nonspecific ion channel to the same total membrane conductance exhibited by the active spiking model at rest and adjusted the reversal potential of this

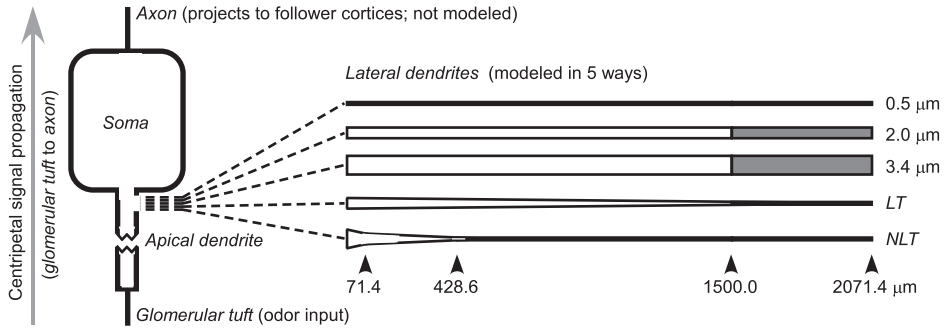

Fig. 1. Model schematic. Afferent signal propagation in MCs begins in the glomerular tuft, proceeding through the apical dendrite and soma (in one of which MC spikes are initiated); these MC spikes then propagate down the axon (centripetally, to higher cortices) and the lateral dendrites (to effect lateral inhibition within the OB). Inhibitory synaptic inputs on these lateral dendrites thus fall outside of the axis of centripetal signal propagation, raising the question of whether and to what extent these synaptic inputs are able to modify olfactory signal propagation to the piriform cortex and other postbulbar structures. Five model dendrites were used to study this question: three of fixed diameter (0.5, 2.0, and 3.4 μm), one linearly tapering (LT), and one realistic, nonlinearly tapering (NLT; see MATERIALS AND METHODS). Except where noted in the text, simulations were performed out to 2,071.4 μm (shaded region), but only analyzed out to 1,500 μm (nonshaded region) to avoid reflection effects due to dendritic caps (ends). The taper of the nonlinearly tapering dendrite changed at 71.4 and 428.6 μm (see MATERIALS AND METHODS).

channel to match the resting potential of the passivized cell to that of the active cell. Consequently, the input resistances and synaptic driving forces of the active (at rest) and passivized cells were identical.

Synaptic Properties

GCs were not explicitly modeled in these simulations; their $GABA_A$ergic synapses onto MCs were modeled only postsynaptically. We modeled the $GABA_A$ergic synapse as a double-exponential function with a rising time constant of 1.25 ms and a decay time constant of 4 ms, consistent with experimental data (Inoue and Strowbridge 2008; Schoppa 2006). Notably, the decay kinetics of $GABA_A$ receptors depend strongly on their α-subunit composition, ranging from 3 ms for receptors containing only α_1-type α-subunits to 30 ms for receptors that contain only α_3. MCs predominantly express receptors with α_1-subunits, as modeled herein, although tufted cells and a superficial subpopulation of MCs express receptors composed of α_3-subunits, or a combination of both (Eyre et al. 2012, Panzanelli et al. 2005).

Variables of Interest

The majority of simulations featured four independent variables: the distance between an inhibitory synapse and the MC soma, the peak conductance of the inhibitory synapse, the diameter of the lateral dendrite, and the (chloride) reversal potential of the $GABA_A$ receptor. In additional studies, we manipulated cellular morphology by gradually tapering or branching the lateral dendrite.

Distance between the inhibitory synapse and the soma. MC lateral dendrites project broadly across the OB EPL and branch several times (Orona et al. 1983), elaborating to a degree sufficient to innervate every column of the OB (Shipley and Ennis 1996). "Column" in the context of the mammalian OB refers to a single glomerulus, the principal neurons (MCs and tufted cells) that innervate it, and the physically neighboring interneurons that interact with them (Cleland 2010). For most simulations in this study, we modeled a single uncapped dendrite of 1,500-μm length (to do this, the actual simulated length of the capped dendrite was 2,071.4 μm, six compartments beyond the end of the region studied; Fig. 1, shaded regions). A dendritic cap refers to the sealed physical end of the dendrite, which accumulates charge that cannot diffuse further, reflecting it back up the dendrite and disrupting the normal exponential decay of potential across distance. Modeling uncapped dendrites avoids this added complication when it is not relevant to the questions being addressed. Where noted, we simulated branching dendrites or modeled the dendrite as capped at 1,500 μm. In all cases, except where specifically noted, the dendritic arbor comprised seven isometric compartments per 500 μm.

Peak synaptic conductance. Based on physiological recordings from MCs, we estimated the peak synaptic conductance for single synaptic events to be on the order of 0.5–2.0 nS, with 10- to 20-nS conductances being representative of coincident synaptic events contributing to a large inhibitory postsynaptic current (Schoppa 2006; Schoppa et al. 1998).

$GABA_A$ receptor reversal potential. The $GABA_A$ receptor fluxes chloride ions and reverses at the ECl, which we modeled at both -70 mV and -78 mV. The -70-mV value is a traditional estimate of ECl in adult animals in vivo and emphasizes shunting effects as it is close to the resting membrane potential (around -69 mV in the passivized models). Experiments in mammalian OB slices, in which ECl is determined by the composition of bath saline, often alter ECl away from the cellular resting potential to better visualize inhibitory synaptic potentials as voltage deflections (Castillo et al. 1999; Pressler and Strowbridge 2006; Schoppa 2006). The -78-mV value reflects the ECl used in many of these slice studies. During development, ECl is often considerably more depolarized than either of these values (Ben-Ari 2002) and sometimes remains so in adult neurons, including OB periglomerular cells, owing to increased intracellular chloride accumulation (Parsa et al. 2014; Siklós et al. 1995; Smith and Jahr 2002). However, these depolarized ECl values have not been observed in adult OB MCs and hence were not simulated.

Diameter of lateral dendrites. The uniform dendritic diameters tested were 0.5 μm, 2.0 μm, and 3.4 μm. MC lateral dendrites taper from roughly 2.0 μm at $\sim$60 μm from the soma (Lowe 2002) to an average of 0.5 μm in diameter at their terminals (Mori et al. 1983). Thus simulations at 2.0-μm diameter are appropriate for estimating the effects of synaptic inputs roughly within a glomerular diameter, while 0.5 μm is the most relevant diameter overall for examining distal synapses. Simulations are also presented using the thicker diameter of the MC apical (primary) dendrite, experimentally estimated at 3–5 μm (Djurisic et al. 2004; Matsutani and Yamamoto 2000) and here modeled as 3.4 μm. Additional simulations incorporated gradually tapering or branching dendrites.

Dendritic tapering. Where noted, simulations were performed on tapering dendrites. Two tapering models were used. In the first, dendrites tapered linearly from 2.0 μm at the soma to 0.5 μm at the end of the dendrite, 1,500 μm distal to the soma (Mori et al. 1983). A more morphologically accurate, nonlinearly tapering model also was constructed. The lateral dendrite in this model tapered from 3.4 to 2.0 μm over the most proximal 71.4 μm, consistent with the tapering measured by Lowe (2002) out to 60 μm from the soma. The dendrite then further tapered from 2.0 to 0.5 μm at a distance of 428.6 μm and maintained a constant 0.5-μm diameter thereafter. These two transition points corresponded to compartment boundaries within the most proximal 500-μm section of the uniform-diameter model dendrites and were selected to maintain odd numbers of compartments per section and to ensure that all computations were performed in identical locations across all models by NEURON (with the sole exception being that the most proximal tapering section was subdivided from one into five compartments to increase spatial resolution). Specifically, the 21 compartments comprising the 1,500-μm dendrite in the nontapered models were reapportioned as follows: 1 to the most proximal tapering section (which then was subdivided into five), 5 to the second tapering section, and 15 to the distal section of constant diameter. Hence, differences in numerical solutions cannot be attributed to artifactual changes in the precise dendritic locations at which differential equations were solved.

Branching. MCs have an estimated average of 6.2 lateral dendrites, each of which branch several times, broadly innervating the extent of the EPL such that each GC could in principle connect with MCs from any glomerulus (Mori et al. 1983; Orona et al. 1983; Shipley and Ennis 1996). We simulated the effects of increased numbers of dendritic branch points to determine the overall effect of branching on the ability of distal synaptic inputs to affect physiological response properties at the soma (presumably by shunting current). In simplified accordance with Mori et al. (1983), we varied the number of branches from 0 to 5, with the first branch point at 100 μm from the soma, and subsequent branches arising at evenly spaced 300-μm intervals (i.e., branch points were at 100, 400, 700, 1,000, and 1,300 μm from the soma). All dendrites in these simulations had a uniform diameter of 2.0 μm to better visualize branching effects.

Properties of the Active Model

The active MC model was taken directly from Li and Cleland (2013) with minimal modification. This model exhibits intrinsic STOs (Desmaisons et al. 1999, Rubin and Cleland 2006) and a full complement of membrane, synaptic, and neuromodulatory currents; supports somatofugal action potential propagation along lateral dendrites; and dynamically synchronizes with other MCs when coupled via GCs in a network resembling that of the OB EPL. Specific membrane capacitance and resistance (at rest) were identical to those in the passivized model, as was R_a. In all active model simulations, the lateral dendrite diameter tapered to match the "morphologically accurate" nonlinear taper described for the passivized model. The peak

conductances of membrane mechanisms were scaled to surface area, just as the corresponding ohmic membrane conductances were in the passivized model.

Dependent Variable Calculation

The effects of inhibitory synaptic inputs on somatic membrane potential were directly measured as the peak deflection from rest. The effects on somatic input resistance were evaluated by opening a current shunt with the same range of conductances as our inhibitory synapses at different sites along the lateral dendrite. We then injected a hyperpolarizing current into the soma and measured the change in somatic membrane potential. Current amplitudes were selected to limit voltage deflections to <5 mV to minimize effects on voltage-dependent currents (when present). We solved for input resistance using Ohm's law.

RESULTS

Passivized Model Definition

Whereas membrane excitation can propagate along axons or active dendrites in the form of action potentials, the effects of inhibitory synaptic inputs do not actively propagate. Hence, it is unclear how or whether inhibitory inputs onto distal regions of MC lateral dendrites are able to affect spike initiation, propagation, or timing at the soma. We first assessed the cable propagation of these inhibitory signals using a "passivized" version of the Li and Cleland (2013) MC model. In this modified model, all membrane conductances were rendered ohmic with total conductances equal to those of the active model at rest (see MATERIALS AND METHODS). Inhibitory synaptic inputs of several different peak conductances were delivered onto the lateral dendrite at distances ranging from 0 to 1,500 μm from the soma. To cover a range of parameters used in existing MC models (Table 1), we employed three different dendritic diameters and two different $GABA_A$ receptor reversal potentials (ECl) in separate simulations. As described in MATERIALS AND METHODS, the single most relevant uniform-diameter parameter set for distal inputs is 0.5-μm diameter with a ECl of −70 mV. A diameter of 2.0 μm is a better approximation for the most proximal ~40–80 μm of dendritic length, roughly within a glomerular diameter, and the alternative ECl of −78 mV better reflects data from most slice recording studies, in which the chloride driving force is often artificially increased to improve inhibitory postsynaptic potential visualization. The largest diameter, 3.4 μm, reflects the size of the MC apical dendrite that connects the glomerular tuft to the MC soma.

Table 1. *Mitral cell model parameters*

Model	R_a, Ω·cm	R_m, Ω·cm^2	C_m, μF/cm^2	E_{leak}, mV
		Passive cell properties		
Current	208	30,000	1.2	varied
Li and Cleland 2013	70	30,000	1.2	−60
David et al. 2008 (long dendrite)	varied	100,000	1	−65
McTavish et al. 2012[a]; Migliore and Shepherd 2008[b]; Migliore et al. 2010[c]; Yu et al. 2013[d]	150	adjusted for R_{in} = 70 MΩ[a,b,c]; R_{in} = 100 MΩ[d]		−65
Shen et al. 1999	70	30,000	1.2	−65
Bhalla and Bower 1993	200	adjusted for R_{in} = 60 MΩ	1	−65
	Length, μm	Diameter, μm	λ, μm	τ_m, ms
		Lateral dendrite properties		
Current	2,071.4	0.5, 2.0, 3.4, linearly tapering, realistically tapering	varied	36
Li and Cleland 2013	500	3.4	1,909	36
David et al. 2008	1,000	17.03	2,675	100
McTavish et al. 2012[a]; Migliore and Shepherd 2008[b]; Migliore et al. 2010[c]; Yu et al. 2013[d]	500[b]; 1,000[a,c]; 1,500[d]	2	171[a,b,c]; 205[d]	20[d]; 30[a,b,c]
Shen et al. 1999	500	3.4	1,909	36
Bhalla and Bower 1993	multiple lateral dendrites of varying sizes and tapers			
	E_{GABA}, mV	τ_{rise}, ms	τ_{decay}, ms	g_{GABA}, nS
		Inhibitory synapse properties		
Current	−70, −78	1.25	4	0.5, 1, 2, 5, 10, 20
Li and Cleland 2013	−80	1.25	18	1.5
David et al. 2008	−70	0	5	varied
McTavish et al. 2012[a]; Migliore and Shepherd 2008[b]; Migliore et al. 2010[c]; Yu et al. 2013[d]	−80	0.1[a]; 1[b,c,d]	4[a]; 200[b,c,d]	1.2 ± 0.4[b]; 3[c,d]; 5[a]

Comparison of parameter values in mitral cell models, including those described herein. Values were obtained from the relevant publications, extracted from the corresponding code on ModelDB (https://senselab.med.yale.edu/ModelDB/), or calculated using cable equations. Not all parameters were relevant to all models. Models sharing a similar basis are grouped together. C_m, specific membrane capacitance; E_{leak}, reversal potential of the leak conductance; E_{GABA}, reversal potential of the GABA-gated synaptic conductance; g_{GABA}, maximum conductance of the GABA receptor channel; R_{in}, empirically measured input resistance; τ_m, membrane time constant; τ_{rise}, onset time constant of the GABA receptor current; τ_{decay}, offset time constant of the GABA receptor current. Other abbreviations are as defined in *Eq. 1*.

Synaptic Effects on Somatic Membrane Potential

$GABA_A$ergic inhibitory synaptic inputs onto the lateral dendrite weakly hyperpolarized the soma in a predictably distance-dependent manner. With an ECl of −70 mV, the polarizing effects were minimal, corresponding to a driving force of 0.1 mV (with 0.5-μm dendrites and a resting potential of −70 mV) to 1.4 mV (with 3.4-μm dendrites and a resting potential of −68.6 mV; Fig. 2, *A–C*). The spike generation threshold for the active model was about −42 mV. Even with a driving force of nearly 10 mV with ECl = −78 mV (Fig. 2, *D–F*), polarizing effects on the soma fell off sharply with distance; synaptic events comparable to one or a few coincident inputs (i.e., 0.5–2.0 nS) generated considerably less than 0.5 mV deflection when located more than a few tens of micrometers from the soma, even given an unrealistically thick dendrite. With a diameter of 0.5 μm, appropriate for dendritic regions more distant than ~100 μm from the soma, even high estimates of total recurrent activity (20 nS) exhibited less than 1 mV deflection when inputs were further than a few tens of micrometers from the soma (roughly 1–2 glomerular diameters). Under the most realistic conditions in vivo (ECl = −70 mV, diameter = 2.0 μm within ~100 μm of soma, 0.5 μm further away; Fig. 2, *A* and *B*), the polarizing effects of synaptic inputs on the soma were negligible. As previously predicted (Cleland 2014; Cleland and Sethupathy 2006; Li and Cleland 2013) and recently experimentally demonstrated (Fukunaga et al. 2014), these results suggest that somatic hyperpolarization via GC inhibition is unlikely to be able to prevent spiking in MCs, particularly when these spikes are initiated within the apical dendrite (Chen et al. 2002).

Synaptic Effects on Somatic Input Resistance

However, polarization is not the only means by which somatic information processing can be affected. Shunting inhibition can sharply affect spike generation, propagation, and timing by transiently reducing the input resistance of particular cellular compartments, even in the absence of membrane polarization (David et al. 2008; Vida et al. 2006). The effects of shunting inhibition also scale with distance along the dendrite, because that distance is effectively a resistor in series with the variable synaptic conductance. However, the efficacy of shunting inhibition on somatic input resistance is insensitive to the synaptic driving force; inhibitory currents with reversal potentials near rest can still strongly affect cellular signaling, even if no voltage deflections are observed. In our simulations, $GABA_A$ergic synaptic inputs onto the lateral dendrite reduced somatic input resistance in a predictably distance-dependent manner (Fig. 3). Dendritic diameter had two prominent effects. First, the baseline MC input resistance decreased with larger dendritic diameters, because the total surface area of the neuron was greater. Second, larger dendritic diameters increased the distance from which synaptic conductances could effectively alter somatic input resistance. A narrow, 0.5-μm-diameter dendrite limited the impact of inhibitory shunt con-

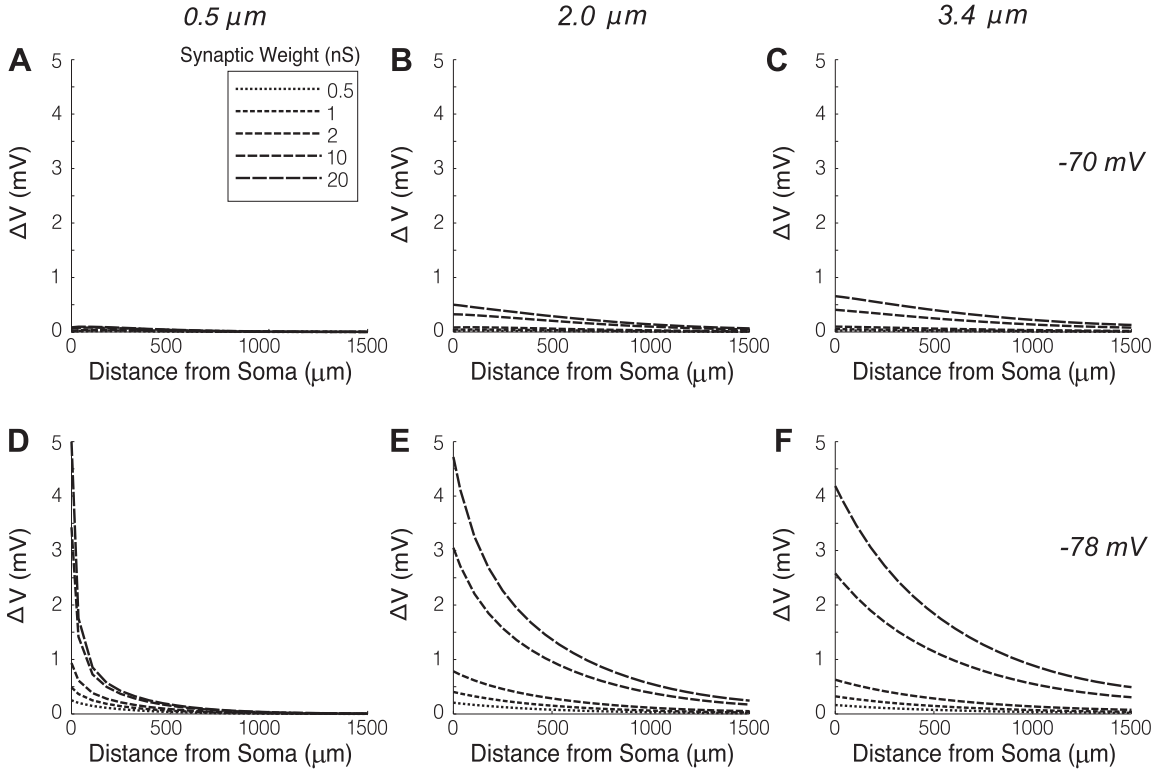

Fig. 2. Changes in the membrane potential of the MC soma (ΔV) in response to inhibitory synaptic inputs along the lateral dendrite. Positive values on the ordinate denote hyperpolarization at the soma. The location of synaptic input ranged from 0 to 1,500 μm from the soma (abscissa). The maximum synaptic conductance was modeled as 0.5, 1, 2, 10, and 20 nS (*inset*); single synaptic events are estimated at 0.5–2.0 nS, with 10- to 20-nS conductances representing reasonable net inhibitory synaptic conductances that can be evoked in MCs by recurrent OB network activity (Schoppa 2006; Schoppa et al. 1998). Simulations were performed using two different chloride reversal potentials (*A–C*: −70 mV; *D–F*: −78 mV; see RESULTS for interpretations) and three lateral dendritic diameters (*A* and *D*: 0.5 μm; *B* and *E*: 2.0 μm; *C* and *F*: 3.4 μm). A diameter of 2.0 μm reflects the most proximal ~40–80 μm of the lateral dendrite, whereas 0.5 μm better reflects its diameter more distally. 3.4 μm reflects the diameter of the primary dendrite and the immediate junction of the lateral dendrite.

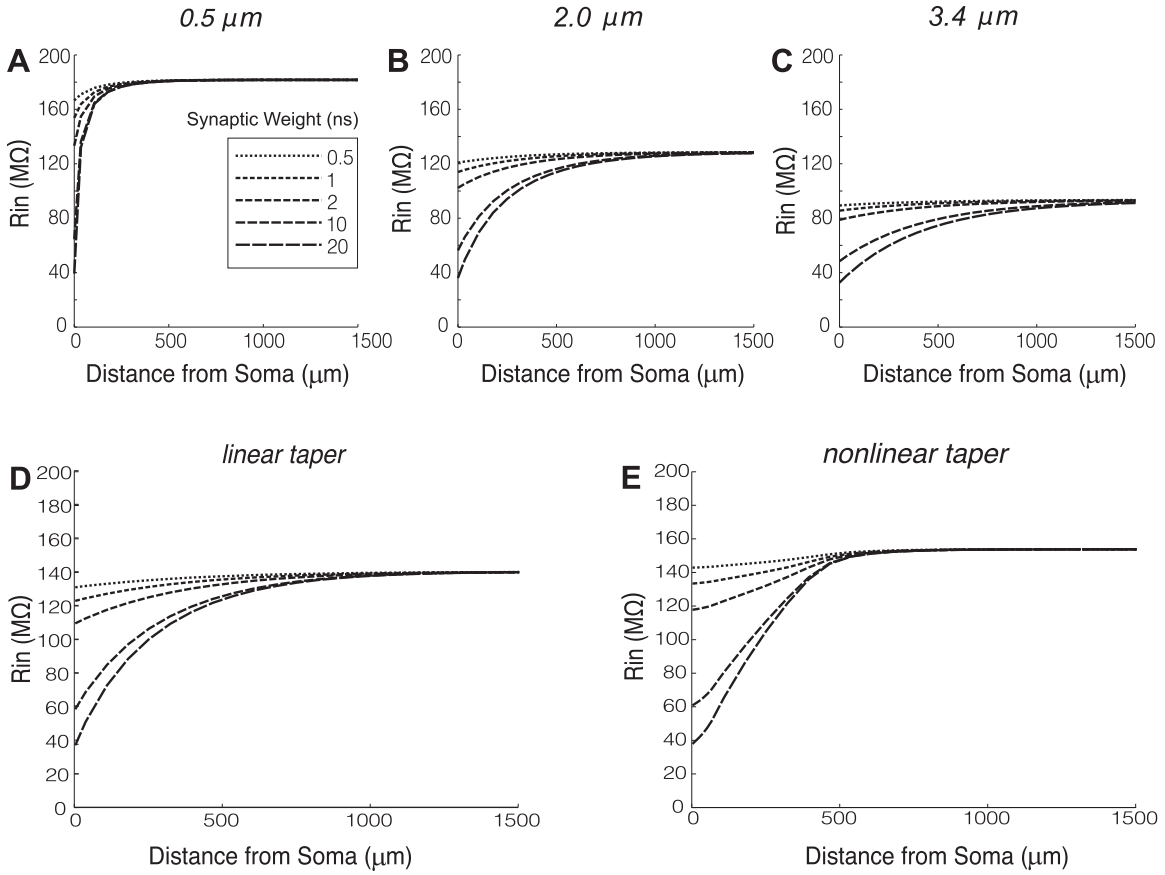

Fig. 3. Changes in somatic input resistance R_{in} with the opening of a shunting conductance along the mitral cell dendrite (abscissa). Five maximum synaptic conductances were modeled (*inset*). R_{in} was measured based on the change in membrane potential in response to a negative square pulse ($\Delta V_{pulse} < 5$ mV) applied to the soma under current clamp conditions. The reversal potential of the shunt was −70 mV, although adjustments to this parameter did not affect results. *A*: 0.5-μm diameter dendrite. *B*: 2.0-μm dendrite. *C*: 3.4-μm dendrite. *D*: linearly tapering dendrite with diameter tapering from 2 μm at the soma to 0.5 μm at 1,500-μm distance (then extending to 2,071.4 μm at a constant 0.5-μm diameter to avoid capping effects). *E*: nonlinearly tapering dendrite with diameter tapering from 3.4 μm at the soma to 2 μm at 71.4-μm distance, then to 0.5 μm at 428.6-μm distance, and then extending to 2,071.4 μm at a constant 0.5-μm diameter to avoid capping effects. See text for details.

ductances to the immediate vicinity of the somatic column (Fig. 3*A*), whereas a 2.0-μm-diameter dendrite enabled somewhat more distal inputs to significantly reduce input resistance at the soma (Fig. 3*B*).

Because the distance at which inhibitory synaptic inputs can effectively modulate somatic signaling is a critical question, and these dendritic diameters differed substantially in the efficacy of their signal propagation, we performed additional simulations using models of tapered dendrites. First, we simulated a simple, linearly tapering dendrite (2.0 μm at the soma, 0.5 μm at 1,500 μm distance; Fig. 3*D*). These simulations exhibited a baseline somatic input resistance between that of the cell with a 0.5-μm-diameter dendrite and that of the cell with a 2.0-μm-diameter dendrite, and a pattern of declining somatic impact with distance similar to that of the cell with a 2.0-μm-diameter dendrite. We then constructed a more complex model of dendritic tapering to more precisely reflect experimental estimates of neuronal morphology. Here, the diameter tapered from 3.4 μm at the soma to 2.0 μm at 71.4-μm distance, then tapered further to 0.5 μm at 428.6-μm distance, and remained at 0.5 μm thereafter (specific values were chosen so as to retain compartment boundaries and locations of computation; Fig. 3*E*). These simulations exhibited sharp limitations on the distances from which inhibitory synaptic inputs are capable of affecting somatic input resistance, while expressing strong responses to proximal synaptic inputs. Overall, the effects of shunting inhibition on somatic input resistance appear quite powerful when the inhibitory synapses are located proximal to the soma, but drop off rapidly with distance. The implication is that even moderately distant synaptic inputs onto MC lateral dendrites may not have sufficient effects on somatic state to affect centripetal spike propagation.

Dendritic Tapering and Capping Effects on Somatic Membrane Potential

Before testing this hypothesis in an active, spiking MC model, we conducted additional simulations with the passivized model to measure the effects of modified morphologies on the capacity of inhibitory synaptic inputs to affect somatic membrane potential. First, using a 2-μm-diameter dendrite (Fig. 4*A*), we capped the dendrite at 1,500 μm in length and observed that distal inputs had a slightly enhanced capacity to hyperpolarize the soma (Fig. 4*B*), although not to a degree likely to exert a meaningful somatic effect. Second, we simulated a linear taper to observe the interaction between the effects of tapering and capping. Using a taper identical to that of Fig. 3*D*, we measured synaptically-induced hyperpolariza-

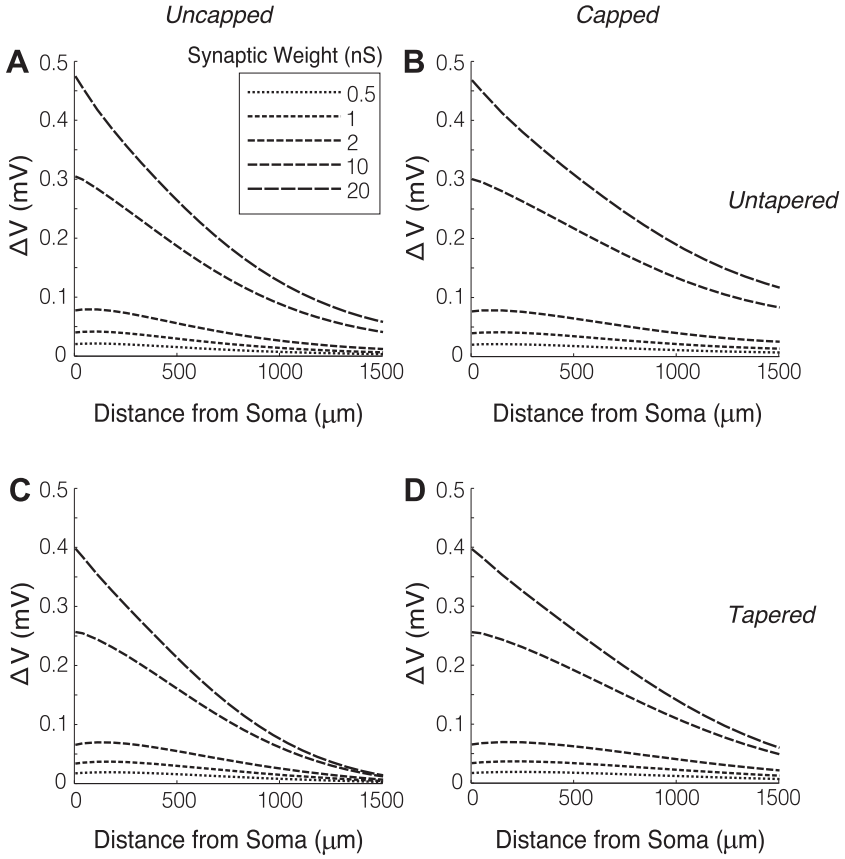

Fig. 4. Comparison of the change in membrane potential at the MC soma (ΔV) in linearly tapered and untapered dendrites, with or without capped ends, in response to inhibitory synaptic input. Synaptic reversal potential was −70 mV. *A* and *B*: 2-μm untapered dendrites. *C* and *D*: dendrites linearly tapered from 2 μm at the soma to 0.5 μm at 1,500 μm along the dendrite. *A* and *C*: uncapped dendrites, generated by simulating out to 2,071.4-μm distance (constant 0.5-μm diameter beyond 1,500-μm distance). *B* and *D*: dendrites capped at 1,500 μm, such that current reflects off of the capped end and marginally enhances efficacy at the soma. Note the change in scale on the ordinate compared with Fig. 1.

tion at the soma along both uncapped (Fig. 4*C*) and capped (Fig. 4*D*) tapering model dendrites. Synapses along a narrowing dendrite had a weaker effect at the soma, whereas capping the dendrite strengthened the somatic effect to roughly the same degree. All other simulations were performed using uncapped dendrites (see MATERIALS AND METHODS) to avoid these effects. Third, we measured the effects of dendritic branching on the capacity of distal inhibitory inputs to affect the soma. Individual MCs extend multiple lateral dendrites into the EPL (mean = 6.2), each of which branches extensively (Orona et al. 1983; Shipley and Ennis 1996). We varied the number of branch points from 0 to 5 and distributed them along the dendrite. To approximate their experimental distribution, as described by Mori et al. (1983), the first branch point was located 100 μm from the soma, and subsequent branches were located at 300-μm intervals thereafter (i.e., branch points were 100, 400, 700, 1,000, and 1,300 μm from the soma). All branches were 2 μm in diameter and untapered. The effect of dendritic branching on MC somatic responses to distal inhibitory inputs was negligible in all cases (Fig. 5).

Active Model Definition

Using the fully active, spiking, dynamic MC model of Li and Cleland (2013), minimally modified (see MATERIALS AND METHODS), we first measured the effects of distal inhibitory synaptic inputs on the membrane potential and input resistance of the MC soma, using variables and methods identical to those employed for the passivized model (Figs. 2 and 3). Results were essentially identical to those observed with the passivized model (data not shown), confirming that the active currents do not play a significant role in the impact of either synaptic inputs or shunting conductances.

The active MC model exhibited STOs in response to the somatic injection of a depolarizing 180-pA current, based on slow internal processes that regulated the timing and burst properties of action potentials. Multiple experimental studies have confirmed that Na^+-dependent STOs occur in MCs, with particular prominence at perithreshold membrane potentials (Balu et al. 2004, Chen and Shepherd 1997, Desmaisons et al. 1999, Heyward et al. 2001). The diameter of the lateral dendrites affected STO and spiking properties; thicker dendrites with their larger membrane surface areas decreased cellular input resistance, reducing the amplitude of the STOs and extending the interburst interval while slightly reducing STO frequency (mean frequency = 38, 34, and 29 Hz with dendrites of diameters 0.5, 2, and 3.4 μm, respectively) (Fig. 6, *A–C*). Burst duration was not affected.

Synaptic Effects on STOs and Spike Timing in the Active Model

Passivized model simulations suggested that synaptic inputs onto MC lateral dendrites that are not closely adjacent to the soma will have little or no effect on somatic state and hence are unlikely to substantially affect spike propagation along the primary neuronal axis. Selecting the complex tapering model described above (Fig. 3*E*) as the most realistic approximation of MC morphology, we tested the capacity of inhibitory synaptic inputs along the lateral dendrite to affect STO properties and spike timing in the active model. The baseline STO frequency and amplitude in the tapered model were similar to

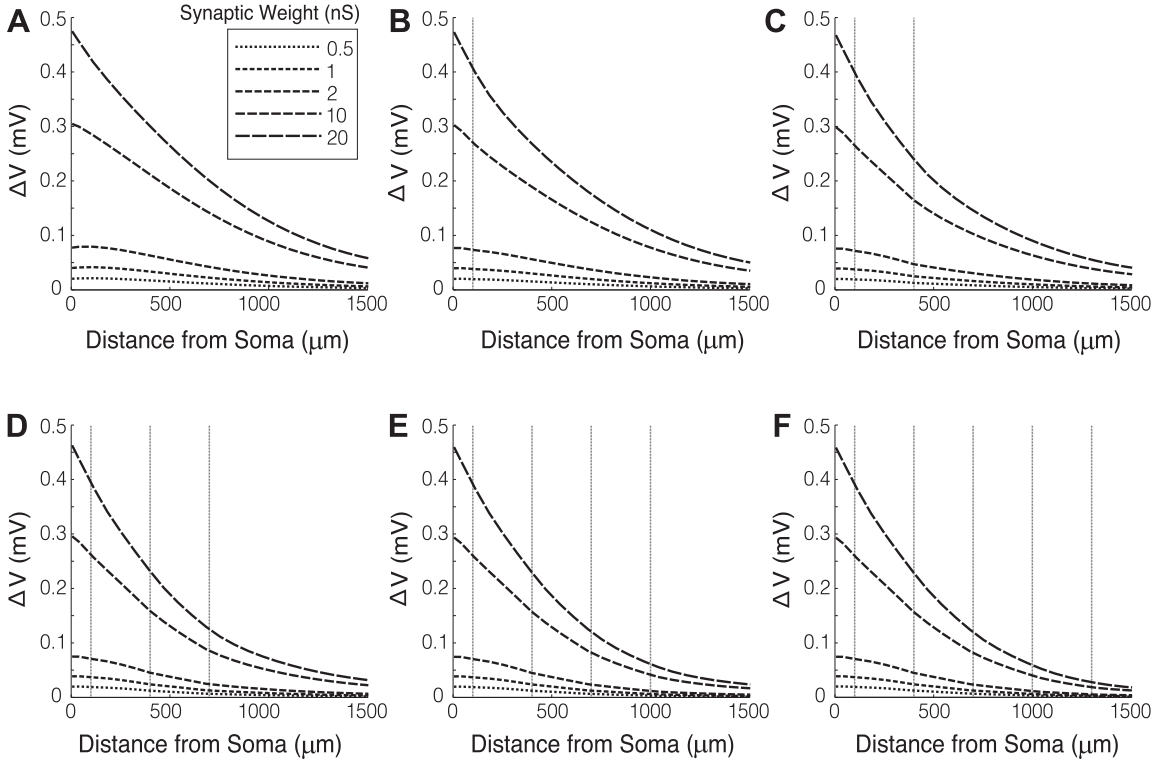

Fig. 5. Comparison of the change in membrane potential at the MC soma (ΔV) in branched and unbranched lateral dendrites. Dendritic diameter was uniform (2 μm) in the main lateral dendrite and across all branches. The number of branches was increased from 0 to 5 (*A* to *F*, respectively), where dashed vertical lines indicate branch points. Branches did not provide additional synaptic inputs. Synaptic reversal potential was −70 mV.

those in the model with an untapered 2.0-μm-diameter dendrite (Fig. 6*D*).

Effects of inhibitory inputs on STOs and spikes in the active model mirrored the passive model results, with distal inputs having no effect on STO or spike timing (Fig. 7). Adjacent to the soma, delays increased with the phase of inhibitory onset, where an STO phase of zero is defined to be the peak of the previous STO. This effect of onset phase on delay suggested that these inhibitory synaptic inputs, delivered in common to multiple MCs, could progressively synchronize their STOs and action potentials. Notably, strong inhibitory or shunting inputs are capable of fully

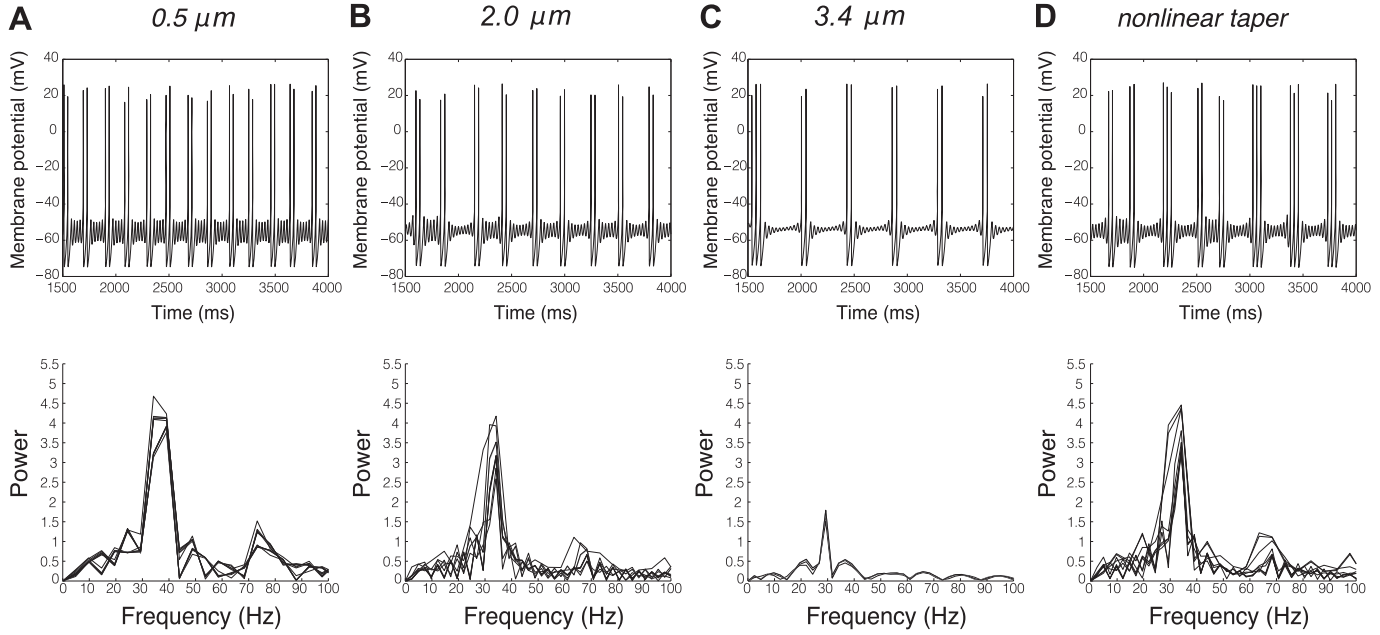

Fig. 6. Active cell model properties. *A–D*, *top*: somatic membrane potential time series in the active MC model alternate bursts of action potentials and interburst intervals exhibiting subthreshold oscillations. *Bottom*: power spectra of subthreshold oscillations within interburst intervals from each corresponding time series. MC lateral dendritic diameters were modeled at four diameters: 0.5 μm (*A*), 2.0 μm (*B*), 3.4 μm (*C*), and nonlinearly tapered from 3.4 to 0.5 μm (*D*), as described in Fig. 2*E* (see MATERIALS AND METHODS). In all cases, activity was generated by 180 pA of depolarizing current injected into the soma.

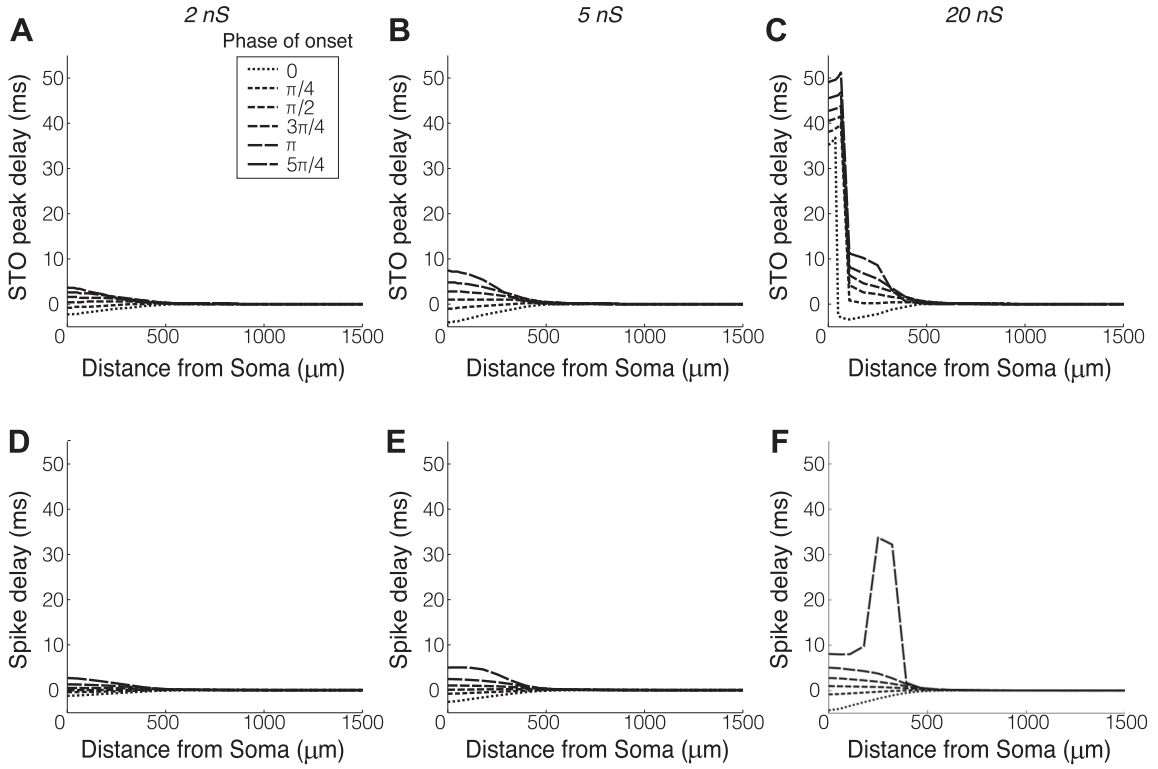

Fig. 7. Effects of inhibitory dendritic synaptic inputs on STO phase and spike timing in the active model MC. The lateral dendrite was nonlinearly tapered (Fig. 1, NLT; see also Figs. 2*E* and 5*D*). *A–C*: lead (negative) or lag (positive) in STO timing induced by inhibitory synaptic inputs delivered at six phases of the original MC STO (*inset*). A zero phase of onset indicates that the onset of the inhibitory postsynaptic current coincided with the somatic STO peak (phase of maximum depolarization). *D–F*: changes in spike timing induced by inhibitory synaptic inputs delivered at six phases of the MC STO immediately preceding the onset of the first spike of a burst. Inputs had a reversal potential of −70 mV and were modeled at three synaptic weights (peak synaptic conductances): 2 nS (*A* and *D*), 5 nS (*B* and *E*), or 20 nS (*C* and *F*). Phases of onset beyond $5\pi/4$ were excluded from the plots as STO peaks were truncated, or spikes skipped (i.e., delayed for at least a full cycle), depending on the strength of input.

resetting the phase of MC STOs (Desmaisons et al. 1999; Li and Cleland 2013; Rubin and Cleland 2006). We, therefore, probed how effectively weaker or more distal synaptic inputs could reset MC STOs and regulate their spike times. $GABA_A$ergic synaptic inputs were first delivered to the lateral dendrite of oscillating MCs during a (nonspiking) interburst interval, at several phases of the STO. Weak inhibitory inputs delivered between STO peaks produced modest shifts in STO timing (Fig. 8*A*). Stronger inputs reduced the effect of phase of onset when delivered proximally to the soma, approaching phase-independent reset (Fig. 8, *B* and *C*), but also could induce rebound spikes when proximal to the soma (Fig. 8*C*). All effects dropped off with increasing distance between synapse and soma.

$GABA_A$ergic synaptic inputs then were delivered at several phases of the final interburst STO just before burst initiation, where they influenced the timing of the subsequent action potential. The effects on spike timing were similar to the effects observed on STO phase resets in the interburst interval (Fig. 8, *D–F*). Specifically, weak inputs exerted minimal effects on spike timing (Fig. 8*D*), whereas stronger effects substantially constrained spike timing with respect to synaptic input, rather than to prior STO phase (Fig. 8*F*), presumably based on the corresponding resetting of the STO phase. Distal inhibitory inputs exerted no measurable effect on MC spike timing, irrespective of their amplitude.

DISCUSSION

Only Proximal Inhibitory Inputs Directly Affect MC Signaling

The simulations described here indicate that lateral inhibitory inputs from GCs onto MC dendrites must be both large and proximal to the MC soma to substantively influence MC centripetal spike propagation. Inputs on the scale of single GC synaptic connections (under 2.0 nS) had minimal effects in these simulations, although there may be substantial periodic background inhibition to MCs in an intact and active network such that a small additional inhibitory conductance, if well-timed, may exert a stronger marginal effect than is illustrated here. In contrast, the effects of distance on inhibitory synaptic efficacy are unmistakable. Whereas inhibitory synapses connect to MC lateral dendrites well over a millimeter away from the MC soma, these distal inhibitory inputs are unable to exert a significant influence on the MC soma, and hence cannot meaningfully influence MC centripetal signaling. Only proximal lateral inhibitory inputs are able to directly influence centripetal information processing within a given MC.

Exactly how proximal to the soma these inputs must be to be functionally effective, however, depends on several parameters that are not precisely known (e.g., R_a) and/or can vary from neuron to neuron (e.g., dendritic tapering). Consequently, in lieu of building a single model with a single set of parameter estimates and drawing conclusions therefrom, we have performed simula-

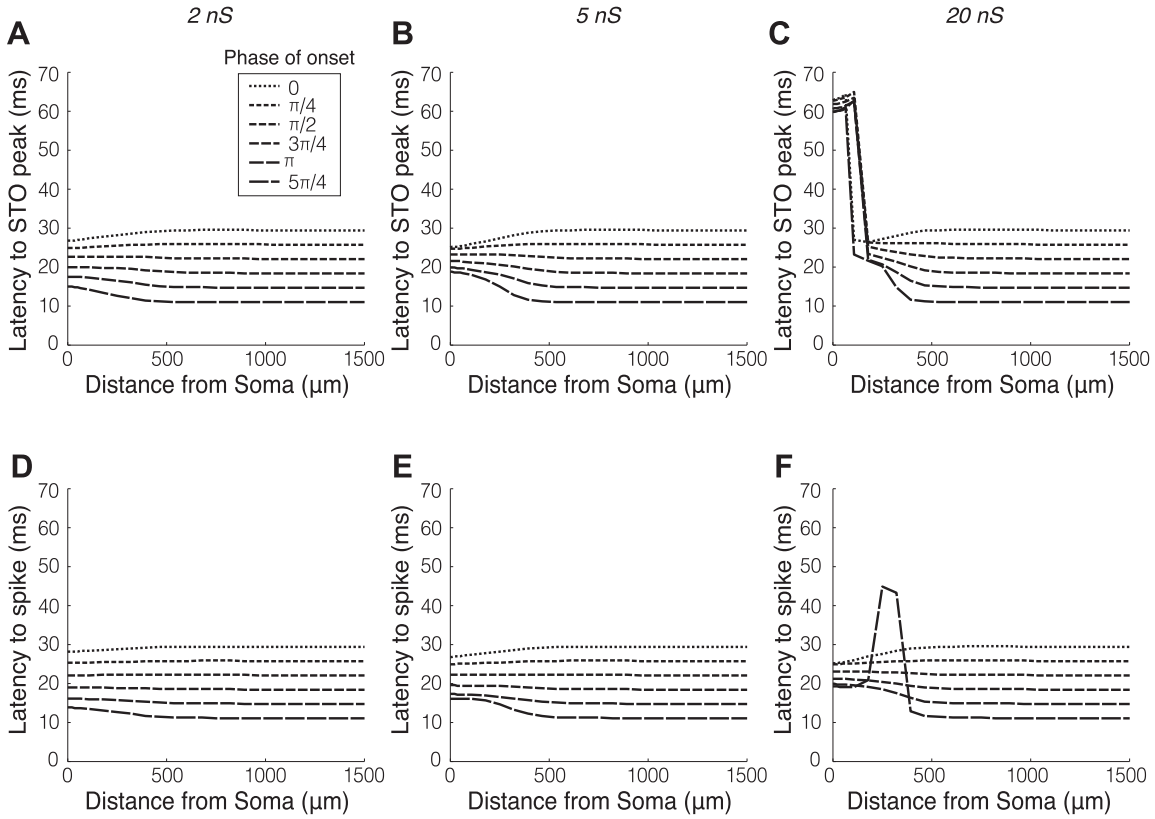

Fig. 8. MC spike timing regulation by inhibitory synaptic inputs and intrinsic STO dynamics. Panels depict the same results shown in Fig. 6, but highlight the constraining effects on MC spike timing. *A–C*: latency between the onset of an inhibitory input delivered to a cell during a nonspiking STO period and the following STO peak. Very strong synaptic inputs delivered adjacent to the soma could induce rebound spikes, substantially delaying the following STO (*C*). *D–F*: latency between the onset of an inhibitory input delivered immediately preceding the onset of a spike burst and the first spike. Multiple phases of onset of the inhibitory synaptic input were tested (*inset*). Inputs had a reversal potential of −70 mV and were modeled at three synaptic weights (peak synaptic conductances): 2 nS (*A* and *D*), 5 nS (*B* and *E*), or 20 nS (*C* and *F*). Phases of onset were defined with 0 as the peak of the preceding STO and 2π as the peak of the following STO or spike in the absence of synaptic input. Phases of onset beyond $5\pi/4$ were excluded from the plots as STO peaks were truncated, or spikes skipped (i.e., delayed for at least a full cycle), depending on the strength of input. Strong inhibitory inputs between two STOs were also capable of triggering rebound spikes and delaying the following STO peak (e.g., *C*). The convergence of the six curves as proximity to the soma increases reflects the degree to which MC STOs are reset to a common phase by inhibitory synaptic input (Rubin and Cleland, 2006).

tions across a range of relevant parameters to illustrate the extent of reasonable uncertainty. These results enable the rejection of some hypotheses, such as the possibility that larger synaptic weights at more distal inputs would be able to compensate for the distance and affect the soma with appreciable efficacy. However, it remains unclear whether inhibitory synapses must be extremely close (such as within a single glomerular diameter of a target MC soma) to be effective, or whether effective inhibition can be delivered from a few hundred micrometers distance.

Lateral Inhibition Affects MC Spike Timing

The efficacy of inhibitory inputs onto MC signaling also depends critically on the metric by which MCs represent information. Inhibitory inputs onto MC lateral dendrites are not well positioned to powerfully suppress MC action potentials, particularly when MC spikes are initiated in the primary dendrite (Chen et al. 2002). Accordingly, contemporary hypotheses propose that GC-MC inhibition primarily affects MC spike timing, and that downstream circuits are constructed to utilize this timing information (Li and Cleland 2013). Indeed, MC spike timing properties contain information about odor quality (Lepousez and Lledo 2013), piriform cortical circuits are responsive to temporally correlated spiking inputs (Davidson and Ehlers 2011; Luna and Schoppa 2008), and traditional olfactory sensory transformations can be performed using spike timing-based computations (Linster and Cleland, 2010). Moreover, MC spikes can be delayed by shunting inhibition, i.e., by reductions in input resistance that dampen membrane excitability, meaning that synaptic reversal potentials near rest (e.g., −70 mV) can deliver effective inhibition in this regime without dependence on membrane hyperpolarization (Figs. 3 and 8) (David et al. 2008). Notably, one class of nestin-positive GCs (type S) directly targets the MC soma and would, therefore, be expected to have particularly strong effects on MC activity (Naritsuka et al. 2009).

We here show that only proximal inhibition onto MC secondary dendrites is effective in delaying MC action potentials. Figure 8 illustrates that proximal inhibitory inputs are able to shift the intrinsic STO phase in MCs to reflect the timing of the inhibitory input, delaying spikes and potentially facilitating the synchronization of MCs that are driven by similarly-timed inhibitory inputs. Stronger inhibitory synaptic inputs can even entirely reset the STO phase in MCs (Li and Cleland 2013; Rubin and Cleland 2006). In related computational work, McTavish and colleagues (2012) demonstrated that only proximal inhibition onto MC lateral dendrites sufficed to synchro-

nize the spiking of MCs coupled to the same GCs, or to synchronous GC populations; distally located inhibitory inputs were ineffective. A corollary of this finding, as also noted by McTavish et al. (2012), is that reciprocal lateral inhibition between two physically distant MCs is most effectively mediated by two separate sets of GCs, each located adjacent to one of the MCs, being excited by the more distant MC, and delivering inhibition onto the proximal MC. This insight is critical for developing and assessing hypotheses of EPL computation and plasticity.

Potential Origin and Roles for Distal Inhibitory Inputs onto MC Lateral Dendrites

MC lateral dendrites form reciprocal dendrodendritic synapses with GABAergic interneurons along their full extents (Bartel et al. 2015; Xiong and Chen 2002). If effective inhibition of MCs by GCs occurs only proximal to MC somata, what is the utility of inhibitory synapses onto distal regions of MC lateral dendrites? One intriguing possibility, originally proposed by Xiong and Chen (2002), is that these synaptic inputs from GCs block action potential propagation along MC lateral dendrites; that is, lateral signaling from a MC to its targets along a particular dendritic branch could be gated by synaptic input from a third-party GC at an intermediate location. Indeed, experimental delivery of inhibition onto MC lateral dendrites via localized puffs of GABA or electrical stimulation of the GC layer successfully blocked somatofugal spike propagation in MC lateral dendrites (Xiong and Chen 2002). However, it remains uncertain whether this gating occurs reliably under natural circumstances, in which inhibitory inputs are likely to be much weaker than these experimental manipulations. Notably, in vivo studies of spike propagation along MC lateral dendrites during odor presentations suggest that local inhibition does not impair propagation, even when dendritic calcium transients are locally attenuated (Debarbieux et al. 2003). Similarly, the local uncaging of GABA along lateral dendrites in vitro can attenuate spike amplitudes locally without impairing their further propagation (Lowe 2002). By analogy with the somatic effects depicted herein, an interesting possibility is that laterally propagating spikes are delayed by mid-dendrite synaptic inhibition, potentially enhancing oscillatory synchrony across the extended network by nonspecifically increasing the coupling density throughout the spatial extent of individual MCs and OB circuitry (Bazhenov et al. 2008; Rulkov and Bazhenov 2008). Not only would this nonspecific-coupling possibility help resolve the serious biophysical problem of how to establish a robust common clock across the OB, necessary for reliable postsynaptic computations based on MC spike timing, but it also bypasses the theoretical problems posed by the specific gating hypothesis. In the OB network, in which physical location correlates neither with chemical quality nor with synaptic connection weights, preventing lateral spike propagation to a set of functionally unrelated neighboring columns targeted by branches of the same MC dendrite is likely to be of limited computational value.

The hypothesis of nonspecific dendrodendritic coupling across the EPL serving to enhance synchronous periodic activity is additionally compatible with recent results, suggesting that many reciprocal synapses located distally on MC lateral dendrites may be formed not with GCs, but with a distinct class of parvalbumin-expressing interneurons, whereas synaptic inputs from GCs are largely proximal to MC somata (Bartel et al. 2015). (Of course, as MC excitation of GCs occurs at great distances, this does not contraindicate the existence of MC-GC synapses, reciprocal or otherwise, at distal dendritic locations.) Parvalbumin-positive (PV+) interneurons have long been proposed to make reciprocal dendrodendritic connections with MC lateral dendrites (Kosaka and Kosaka 2008; Toida et al. 1994); more recent work has indicated that these neurons connect broadly across MCs, in contrast to the apparent specificity of GC connections (Kato et al. 2013; Miyamichi et al. 2013). Evidence that GABAergic feedback inhibition onto MC lateral dendrites does not require GC spiking (Isaacson and Strowbridge 1998; Schoppa et al. 1998) is likely to also apply to PV+ interneurons. The putative spatial segregation of these reciprocal synapses on MCs into proximal (GC) and distal (PV+) subtypes suggests a functional division of labor: a dense but nonspecific dendrodendritic synaptic network based on MC-PV+ interactions that generates and maintains a dynamic clock across the EPL network, while a sparse and specifically targeted synaptic network based on MC-GC interactions underlies intercolumnar lateral inhibition, strongly shaped by learning and mediated largely by spike timing delays within the structure of this common clock. This segregation, if corroborated by future studies, may help resolve a number of subtle but biophysically critical problems in OB computational modeling, including the problem of maintaining coherence across a physically large network coupled by delay lines with short-length constants and a wide distribution of lengths and the problem of generating a reliable baseline of periodic inhibition in the gamma band based solely on GABAergic synaptic inputs that are fast, sparse, and plastic.

Summary

The computations performed by MCs and GCs in the OB EPL have been a central question in olfactory neuroscience for decades (Rall et al. 1966). Establishing a theory to describe the topology of their interactions (e.g., effective inhibition must be delivered proximally to the MC soma) and the mechanism by which MC signaling properties are modified (e.g., by delaying centripetal action potentials with respect to a common oscillatory clock) is necessary before addressing narrower questions, such as the implications of learning-associated synaptic weight changes or the incorporation of adult-generated neurons into OB circuitry.

ACKNOWLEDGMENTS

The authors thank Dr. Guoshi Li for early consultations.

GRANTS

This work was supported by National Institute on Deafness and Other Communications Disorders Rearch Grants R01 DC014701 and R01 DC014367 to T. A. Cleland. Support for A. B. R. McIntyre was provided by the Tri-Institutional Training Program in Computational Biology and Medicine.

DISCLOSURES

No conflicts of interest, financial or otherwise, are declared by the author(s).

AUTHOR CONTRIBUTIONS

A.B.R.M. performed experiments; A.B.R.M. analyzed data; A.B.R.M. and T.A.C. interpreted results of experiments; A.B.R.M. and T.A.C. prepared figures; A.B.R.M. and T.A.C. drafted manuscript; A.B.R.M. and T.A.C. edited and revised manuscript; A.B.R.M. and T.A.C. approved final version of manuscript; T.A.C. conception and design of research.

REFERENCES

Arruda-Carvalho M, Akers KG, Guskjolen A, Sakaguchi M, Josselyn SA, Frankland PW. Posttraining ablation of adult-generated olfactory granule cells degrades odor-reward memories. *J Neurosci* 34: 15793–15803, 2014.

Balu R, Larimer P, Strowbridge BW. Phasic stimuli evoke precisely timed spikes in intermittently discharging mitral cells. *J Neurophysiol* 92: 743–753, 2004.

Bartel D, Rela L, Hsieh L, Greer C. Dendrodendritic synapses in the mouse olfactory bulb external plexiform layer. *J Comp Neurol* 523: 1145–1161, 2015.

Bazhenov M, Rulkov N, Timofeev I. Effect of synaptic connectivity on long-range synchronization of fast cortical oscillations. *J Neurophysiol* 100: 1562–1575, 2008.

Ben-Ari Y. Excitatory actions of GABA during development: the nature of the nurture. *Nat Rev Neurosci* 3: 728–739, 2002.

Bhalla US, Bower JM. Exploring parameter space in detailed single neuron models: simulations of the mitral and granule cells of the olfactory bulb. *J Neurophysiol* 69: 1948–1965, 1993.

Castillo PE, Carleton A, Vincent JD, Lledo PM. Multiple and opposing roles of cholinergic transmission in the main olfactory bulb. *J Neurosci* 19: 9180–9191, 1999.

Chen WR, Shen GY, Shepherd GM, Hines ML, Midtgaard J. Multiple modes of action potential initiation and propagation in mitral cell primary dendrite. *J Neurophysiol* 88: 2755–2764, 2002.

Chen WR, Shepherd GM. Membrane and synaptic properties of mitral cells in slices of rat olfactory bulb. *Brain Res* 745: 189–196, 1997.

Christie JM, Westbrook GL. Regulation of backpropagating action potentials in mitral cell lateral dendrites by A-type potassium currents. *J Neurophysiol* 89: 2466–2472, 2003.

Cleland TA. Construction of odor representations by olfactory bulb microcircuits. *Prog Brain Res* 208: 177–203, 2014.

Cleland TA. Early transformations in odor representation. *Trends Neurosci* 33: 130–139, 2010.

Cleland TA, Sethupathy P. Non-topographical contrast enhancement in the olfactory bulb. *BMC Neurosci* 7: 7, 2006.

David F, Linster C, Cleland TA. Lateral dendritic shunt inhibition can regularize mitral cell spike patterning. *J Comput Neurosci* 25: 25–38, 2008.

Davidson I, Ehlers M. Neural circuit mechanisms for pattern detection and feature combination in olfactory cortex. *Neuron* 70: 82–94, 2011.

Debarbieux F, Audinat E, Charpak S. Action potential propagation in dendrites of rat mitral cells in vivo. *J Neurosci* 23: 5553–5560, 2003.

Desmaisons D, Vincent JD, Lledo PM. Control of action potential timing by intrinsic subthreshold oscillations in olfactory bulb output neurons. *J Neurosci* 19: 10727–10737, 1999.

Djurisic M, Antic S, Chen WR, Zecevic D. Voltage imaging from dendrites of mitral cells: EPSP attenuation and spike trigger zones. *J Neurosci* 24: 6703–6714, 2004.

Eyre MD, Renzi M, Farrant M, Nusser Z. Setting the time course of inhibitory synaptic currents by mixing multiple GABAA receptor α subunit isoforms. *J Neurosci* 32: 5853–5867, 2012.

Fantana AL, Soucy ER, Meister M. Rat olfactory bulb mitral cells receive sparse glomerular inputs. *Neuron* 59: 802–814, 2008.

Fukunaga I, Herb JT, Kollo M, Boyden ES, Schaefer AT. Independent control of gamma and theta activity by distinct interneuron networks in the olfactory bulb. *Nat Neurosci* 17: 1208–1216, 2014.

Heyward P, Ennis M, Keller A, Shipley MT. Membrane bistability in olfactory bulb mitral cells. *J Neurosci* 21: 5311–5320, 2001.

Inoue T, Stowbridge BW. Transient activity induces a long-lasting increase in the excitability of olfactory bulb interneurons. *J Neurophysiol* 99: 187–199, 2008.

Isaacson JS, Stowbridge BW. Olfactory reciprocal synapses: dendritic signaling in the CNS. *Neuron* 20: 749–761, 1998.

Kato H, Gillet S, Peters A, Isaacson JS, Komiyama T. Parvalbumin-expressing interneurons linearly control olfactory bulb output. *Neuron* 80: 1218–1231, 2013.

Kosaka T, Kosaka K. Heterogeneity of parvalbumin-containing neurons in the mouse main olfactory bulb, with special reference to short-axon cells and betaIV-spectrin positive dendritic segments. *Neurosci Res* 60: 56–72, 2008.

Lepousez G, Lledo PM. Odor discrimination requires proper olfactory fast oscillations in awake mice. *Neuron* 80: 1010–1024, 2013.

Lepousez G, Valley MT, Lledo PM. The impact of adult neurogenesis on olfactory bulb circuits and computations. *Annu Rev Physiol* 75: 339–363, 2013.

Li G, Cleland TA. A two-layer biophysical model of cholinergic neuromodulation in olfactory bulb. *J Neurosci* 33: 3037–3058, 2013.

Linster C, Cleland TA. Decorrelation of odor representations via spike timing-dependent plasticity. *Front Comput Neurosci* 4: 157, 2010.

Lowe G. Inhibition of backpropagating action potentials in mitral cell secondary dendrites. *J Neurophysiol* 88: 64–85, 2002.

Luna V, Schoppa NE. GABAergic circuits control input-spike coupling in the piriform cortex. *J Neurosci* 28: 8851–8859, 2008.

Matsutani S, Yamamoto N. Differentiation of mitral cell dendrites in the developing main olfactory bulbs of normal and naris-occluded rats. *J Comp Neurol* 418: 402–410, 2000.

McTavish TS, Migliore M, Shepherd GM, Hines ML. Mitral cell spike synchrony modulated by dendrodendritic synapse location. *Front Comput Neurosci* 6: 3, 2012.

Migliore M, Shepherd GM. Dendritic action potentials connect distributed dendrodendritic microcircuits. *J Comput Neurosci* 24: 207–221, 2008.

Migliore M, Hines ML, McTavish TS, Shepherd GM. Functional roles of distributed synaptic clusters in the mitral-granule cell network of the olfactory bulb. *Front Integr Neurosci* 4: 122, 2010.

Miyamichi K, Shlomai-Fuchs Y, Shu M, Weissbourd B, Luo L, Mizrahi A. Dissecting local circuits: parvalbumin interneurons underlie broad feedback control of olfactory bulb output. *Neuron* 80: 1232–1245, 2013.

Mori K, Kishi K, Ojima H. Distribution of dendrites of mitral, displaced mitral, tufted, and granule cells in the rabbit olfactory bulb. *J Comp Neurol* 219: 339–355, 1983.

Naritsuka H, Sakai K, Hashikawa T, Mori K, Yamaguchi M. Perisomatic-targeting granule cells in the mouse olfactory bulb. *J Comp Neurol* 515: 409–426, 2009.

Orona E, Rainer EC, Scott JW. Dendritic and axonal organization of mitral and tufted cells in the rat olfactory bulb. *J Comp Neurol* 226: 346–356, 1984.

Orona E, Scott JW, Rainer EC. Different granule cell populations innervate superficial and deep regions of the external plexiform layer in rat olfactory bulb. *J Comp Neurol* 217: 227–237, 1983.

Panzanelli P, Perazzini AZ, Fritschy JM, Sassoè-Pognetto M. Heterogeneity of γ-aminobutyric acid type A receptors in mitral and tufted cells of the rat main olfactory bulb. *J Comp Neurol* 484: 121–131, 2005.

Parsa P, D'Souza RD, Vijayaraghavan S. Amplification of nicotinic receptor-mediated glomerular inhibition by signaling between periglomerular cells in the mouse olfactory bulb (Abstract). *Soc Neurosci Abstr* 719: 23, 2014.

Pressler RT, Stowbridge BW. Blanes cells mediate persistent feedforward inhibition onto granule cells in the olfactory bulb. *Neuron* 49: 889–904, 2006.

Rall W, Shepherd GM, Reese TS, Brightman MW. Dendrodendritic synaptic pathway for inhibition in the olfactory bulb. *Exp Neurol* 14: 44–56, 1966.

Rubin DB, Cleland TA. Dynamical mechanisms of odor processing in olfactory bulb mitral cells. *J Neurophysiol* 96: 555–568, 2006.

Rulkov N, Bazhenov M. Oscillations and synchrony in large-scale cortical network models. *J Biol Phys* 34: 279–299, 2008.

Schoppa NE. Synchronization of olfactory bulb mitral cells by precisely timed inhibitory inputs. *Neuron* 49: 271–283, 2006.

Schoppa NE, Kinzie JM, Sahara Y, Segerson TP, Westbrook GL. Dendrodendritic inhibition in the olfactory bulb is driven by NMDA receptors. *J Neurosci* 18: 6790–6802, 1998.

Shen GY, Chen WR, Midtgaard J, Shepherd GM, Hines ML. Computational analysis of action potential initiation in mitral cell soma and dendrites based on dual patch recordings. *J Neurophysiol* 82: 3006–3020, 1999.

Shipley MT, Ennis M. Functional organization of olfactory system. *J Neurobiol* 30: 123–176, 1996.

Siklós L, Rickmann M, Joó F, Freeman WJ, Wolff JR. Chloride is preferentially accumulated in a subpopulation of dendrites and periglomerular cells of the main olfactory bulb in adult rats. *Neuroscience* 1: 165–172, 1995.

Smith TC, Jahr CE. Self-inhibition of olfactory bulb neurons. *Neuroscience* 5: 760–766, 2002.

Soucy ER, Albeanu DF, Fantana AL, Murthy VN, Meister M. Precision and diversity in an odor map on the olfactory bulb. *Nat Neurosci* 12: 210–220, 2009.

Toida K, Kosaka K, Heizmann C, Kosaka T. Synaptic contacts between mitral/tufted cells and GABAergic neurons containing calcium-binding protein parvalbumin in the rat olfactory bulb, with special reference to reciprocal synapses between them. *Brain Res* 650: 347–352, 1994.

Tong MT, Peace ST, Cleland TA. Properties and mechanisms of olfactory learning and memory. *Front Behav Neurosci* 8: 238, 2014.

Vida I, Bartos M, Jonas P. Shunting inhibition improves robustness of gamma oscillations in hippocampal interneuron networks by homogenizing firing rates. *Neuron* 49: 107–117, 2006.

Xiong W, Chen WR. Dynamic gating of spike propagation in the mitral cell lateral dendrites. *Neuron* 34: 115–126, 2002.

Yokoi M, Mori K, Nakanishi S. Refinement of odor molecule tuning by dendrodendritic synaptic inhibition in the olfactory bulb. *Proc Natl Acad Sci U S A* 92: 3371–3375, 1995.

Yu Y, McTavish TS, Hines ML, Shepherd GM, Valenti C, Migliore M. Sparse distributed representation of odors in a large-scale olfactory bulb circuit. *PLoS Comput Biol* 9: e1003014, 2013.